Syntheses, Structure, Magnetism, and Optical Properties of the Interlanthanide Sulfides δ-$Ln_{2-x}Lu_xS_3$ (Ln = Ce, Pr, Nd)

Geng Bang Jin,[†] Eun Sang Choi,[‡] Robert P. Guertin,[§] James S. Brooks,[‡] Travis H. Bray,[†] Corwin H. Booth,[£] and Thomas E. Albrecht-Schmitt[†,*]

[†]Department of Chemistry and Biochemistry and the E. C. Leach Nuclear Science Center, Auburn University, Auburn, Alabama 36849

[‡]Department of Physics and National High Magnetic Field Laboratory, Florida State University, Tallahassee, Florida 32310

[§]Department of Physics and Astronomy, Tufts University, Medford, Massachusetts 02155

[£]Chemical Sciences Division, Lawrence Berkeley National Laboratory, 1 Cyclotron Rd., Berkeley, CA 94720

Published in Journal of Solid State Chemistry ***180****, 2129 (2007).*

Abstract

δ-$Ln_{2-x}Lu_xS_3$ (Ln = Ce, Pr, Nd; x = 0.67 – 0.71) compounds have been synthesized through the reaction of elemental rare earth metals and S using Sb_2S_3 flux at 1000 °C. These compounds are isotypic with $CeTmS_3$, which has a complex three-dimensional structure. It includes four larger Ln^{3+} sites in eight- and nine-coordinate environments, two disordered seven-coordinate Ln^{3+}/Lu^{3+} positions, and two six-coordinate Lu^{3+} ions. The structure is constructed from one-dimensional chains of LnS_n (n = 6 – 9) polyhedra that extend along the *b* axis. These polyhedra share faces or edges with two neighbors within the chains, while in the [*ac*] plane they share edges and corners with other chains. Least square refinements gave rise to the formulas of δ-$Ce_{1.30}Lu_{0.70}S_3$, δ-$Pr_{1.29}Lu_{0.71}S_3$ and δ-$Nd_{1.33}Lu_{0.67}S_3$, which are consistent with the EDX analysis and magnetic susceptibility data. δ-$Ln_{2-x}Lu_xS_3$ (Ln = Ce, Pr, Nd; x = 0.67 – 0.71) show no evidence of magnetic ordering down to 5 K. Optical properties measurements show that the band gaps for δ-$Ce_{1.30}Lu_{0.70}S_3$, δ-$Pr_{1.29}Lu_{0.71}S_3$, and δ-$Nd_{1.33}Lu_{0.67}S_3$ are 1.25 eV, 1.38 eV, and 1.50 eV, respectively. Crystallographic data: δ-$Ce_{1.30}Lu_{0.70}S_3$, monoclinic, space group $P2_1/m$, a = 11.0186(7), b = 3.9796(3), c = 21.6562(15) Å, β = 101.6860(10), V = 929.93(11), Z = 8; δ-$Pr_{1.29}Lu_{0.71}S_3$, monoclinic, space group $P2_1/m$, a = 10.9623(10), b = 3.9497(4), c = 21.5165(19) Å, β = 101.579(2), V = 912.66(15), Z = 8; δ-$Nd_{1.33}Lu_{0.67}S_3$, monoclinic, space group $P2_1/m$, a = 10.9553(7), b = 3.9419(3), c = 21.4920(15) Å, β = 101.5080(10), V = 909.47(11), Z = 8.

Introduction

Ternary interlanthanide chalcogenides display a wide variety of structures that can possess both ordered and disordered Ln^{3+} sites [1-14]. The ordering of two different Ln^{3+} cations over two or more crystallographic sites can be achieved by maximizing the difference in the size of the Ln^{3+} ions. Typical examples of ordered phases include α-$LnLn'S_3$ ($GdFeO_3$-type [15]) [1-4], β-$LnLn'Q_3$ (Q = S, Se) ($UFeS_3$-type [16]) [3, 5, 6], and γ-$LnLn'S_3$ [7]. In these compounds, there are sharp demarcations in coordination numbers and bond distances between the larger ions and smaller ions, which inhibit the disordering of two lanthanides. In contrast, mixed site occupancies are found in disordered structures, e.g. F-Ln_2S_3 ($CeYb_3S_6$ [9]) [17, 18], $CeTmS_3$ [10], and Y_5S_7 ($Sc_2Er_3S_7$ [11]) [19]. When the difference in size between the two Ln^{3+} ions becomes too small, disorder is unavoidable owing to the strong similarities in the structural chemistry of lanthanides. This is best represented by F-Ln_2S_3 type compounds, which contain an eight-coordinate environment for larger Ln^{3+} ion (A), a seven-coordinate intermediate site (B), and two six-coordinate octahedral sites for the smaller Ln^{3+} ion (C). In case of F-$GdLu_3S_6$, the position B is occupied by both metal ions [9]. For F-Er_3ScS_6, both C sites are disordered [8].

In addition to the remarkable structural flexibility of mixed-lanthanide sulfides that gives rise to a myriad of structure types, these compounds also display important physical properties including tunable band gaps. In an effort to understand the structure-property relationships in interlanthanide chalcogenides, we present the preparation,

structure determination, magnetism, and optical properties of the partially disordered δ-$Ln_{2-x}Lu_xS_3$ (Ln = Ce, Pr, Nd; x = 0.67 – 0.71) ($CeTmS_3$-type) compounds.

Experimental

Starting Materials. Ce (99.9%, Alfa-Aesar), Pr (99.9%, Alfa-Aesar), Nd (99.9%, Alfa-Aesar), Lu (99.9%, Alfa-Aesar), S (99.5%, Alfa-Aesar), and Sb (99.5%, Alfa-Aesar) were used as received. The Sb_2S_3 flux was prepared from the direct reaction of the elements in sealed fused-silica ampoules at 850 °C.

Syntheses of δ-$Ln_{2-x}Lu_xS_3$ (Ln = Ce, Pr, Nd; x = 0.67 – 0.71). Reaction mixtures included 0.2000 g of Ln, Lu, S, and Sb_2S_3 in a ratio of 1:1:3:0.5 mmol. They were loaded into fused-silica ampoules in an argon-filled glovebox. The ampoules were sealed under vacuum and heated in the following profile using a programmable tube furnace.: 2 °C/min to 500 °C (held for 1 h), 0.5 °C/min to 1000 °C (held for 5 d), 0.04 °C/min to 550 °C (held for 2 d), and 0.5 °C/min to 24 °C. High yields of black crystals of δ-$Ce_{1.30}Lu_{0.70}S_3$ and dark red crystals of δ-$Pr_{1.29}Lu_{0.71}S_3$ and δ-$Nd_{1.33}Lu_{0.67}S_3$ were isolated manually. Powder X-ray diffraction measurements were used to confirm phase purity by comparing the powder patterns calculated from the single crystal X-ray structures with the experimental data. Semi-quantitative SEM/EDX analyses were performed using a JEOL 840/Link Isis or JEOL JSM-7000F instruments. Ln, Ln', and S percentages were calibrated against standards. Sb was not detected in the crystals. The Ln:Ln':S ratios were determined to be approximately 2:1:4.5 from EDX analyses.

Crystallographic Studies. Single crystals of δ-$Ln_{2-x}Lu_xS_3$ (Ln = Ce, Pr, Nd; x =

0.67 – 0.71) were mounted on glass fibers with epoxy and optically aligned on a Bruker APEX single crystal X-ray diffractometer using a digital camera. Initial intensity measurements were performed using graphite monochromated Mo Kα (λ = 0.71073 Å) radiation from a sealed tube and monocapillary collimator. SMART (v 5.624) was used for preliminary determination of the cell constants and data collection control. The intensities of reflections of a sphere were collected by a combination of 3 sets of exposures (frames). Each set had a different ϕ angle for the crystal and each exposure covered a range of 0.3° in ω. A total of 1800 frames were collected with exposure times per frame of 10 or 20 seconds depending on the crystal.

For δ-$Ln_{2-x}Lu_xS_3$ (Ln = Ce, Pr, Nd; x = 0.67 – 0.71), determination of integrated intensities and global refinement were performed with the Bruker SAINT (v 6.02) software package using a narrow-frame integration algorithm. These data were treated first with a face-indexed numerical absorption correction using XPREP [20], followed by a semi-empirical absorption correction using SADABS [21]. The program suite SHELXTL (v 6.12) was used for space group determination (XPREP), direct methods structure solution (XS), and least-squares refinement (XL) [20]. The final refinements included anisotropic displacement parameters for all atoms and secondary extinction. Some crystallographic details are given in Table 1. Atomic coordinates and equivalent isotropic displacement parameters for δ-$Ln_{2-x}Lu_xS_3$ (Ln = Ce, Pr, Nd; x = 0.67 – 0.71) are given in Tables 2-4. Additional crystallographic details can be found in the Supporting Information.

The structure of $CeTmS_3$ was previously determined to be ordered, with four eight-coordinate Ce^{3+} ions, two seven-coordinate Tm^{3+} and two six-coordinate Tm^{3+} ions

[10]. However, elemental analysis for δ-$Ln_{2-x}Lu_xS_3$ (Ln = Ce, Pr, Nd; x = 0.67 – 0.71) indicated the ratio of Ln^{3+}: Lu^{3+} is approximately 2:1. Considerable disordering of Ce/Lu in the Lu^{3+} positions should be present. Reexamining the Tm-S bond distances in $CeTmS_3$, the average values of $Tm(3)S_7$ and $Tm(4)S_7$ are 2.77 and 2.86 Å respectively. Compared to the Shannon's data [22], in which TmS_7 and CeS_7 are 2.77 and 2.91 Å, Tm(4) site is more likely disordered. For δ-$Ln_{2-x}Lu_xS_3$ (Ln = Ce, Pr, Nd; x = 0.67 – 0.71), the four eight-coordinate positions were assigned as Ln^{3+} and the Tm(1), Tm(2) and Tm(3) sites were assigned as Lu^{3+} at the beginning of the refinement cycles. Two large residual electron density peaks approximately 0.5 Å away from each other were found in the original place of Tm(4). Each of these sites was assigned as Ln^{3+} positions. The one with longer Ln-S bond distances was named as Ln(5) (Ln = Ce, Pr, or Nd), and the other one was assigned as Lu(4). It has to be mentioned, switching the Ln(5) and Lu(4) positions as well as disordering of Ln(5)/Lu(4) at one site were both tried, and gave poorer residuals. The refinement of occupancies of Ln(5) and Lu(4) showed 3:2 ratio of Ln^{3+}:Lu^{3+}, which requires more disordering in other Lu^{3+} sites. In the next step, Ln/Lu were both assigned at Lu(3) positions. This lowered the R_1 value and the weighting scheme to an even greater extent. The final refinements gave rise to formulas of δ-$Ce_{1.30}Lu_{0.70}S_3$, δ-$Pr_{1.29}Lu_{0.71}S_3$, and δ-$Nd_{1.33}Lu_{0.67}S_3$, which are consistent with the Ln:Lu ratios from calibrated EDX results. The standard deviation on the composition from the refinements is 0.01.

Powder X-ray Diffraction. Powder X-ray diffraction patterns were collected with a Rigaku Miniflex powder X-ray diffractometer using Cu Kα (λ = 1.54056 Å) radiation.

Magnetic Susceptibility Measurements. Magnetism data were measured on powders in gelcap sample holders with a Quantum Design MPMS 7T magnetometer/susceptometer between 2 and 300 K and in applied fields up to 7 T. DC susceptibility measurements were made under zero-field-cooled conditions with an applied field of 0.1 T. Susceptibility values were corrected for the sample diamagnetic contribution according to Pascal's constants [23] as well as for the sample holder diamagnetism. θ_p values were obtained from extrapolations from fits between 100 and 300 K. In addition, ZFC and FC data were collected as follows: The samples were first zero field cooled from room temperature and the susceptibility was measured at 100 Oe to 300 K. Then the sample was field cooled at 100 Oe to 2 K and the same measurement was done by increasing with increasing temperatures. There are no differences between ZFC and FC data at the measured temperatures.

UV-vis-NIR Diffuse Reflectance Spectroscopy. The diffuse reflectance spectra for δ-$Ln_{2-x}Lu_xS_3$ (Ln = Ce, Pr, Nd; x = 0.67 – 0.71) were measured from 200 to 1500 nm using a Shimadzu UV3100 spectrophotometer equipped with an integrating sphere attachment. The Kubelka-Munk function was used to convert diffuse reflectance data to absorption spectra [24].

Results and Discussion

Structures of δ-$Ln_{2-x}Lu_xS_3$ (Ln = Ce, Pr, Nd; x = 0.67 – 0.71). The δ-$Ln_{2-x}Lu_xS_3$ (Ln = Ce, Pr, Nd; x = 0.67 – 0.71) series are isotypic with $CeTmS_3$ [10], which crystallizes in $P2_1/m$ space group with a very complex three-dimensional structure. A view of the unit cell is illustrated in Figure 1. There are nine crystallographically unique

lanthanides sites and twelve sulfide positions. Ln(1) are coordinated to nine S atoms in a tricapped trigonal prismatic environment with two long capping Ln···S contacts. For instance, in δ-$Ce_{1.30}Lu_{0.70}S_3$ the short Ce-S bond distances range from 2.8940(19) Å to 3.025(3) Å, while the longer contacts are 3.476(3) Å and 3.957(3) Å. The longest of these can probably be disregarded. Ln(2), Ln(3), and Ln(4) have similar coordination geometries. All of them bond to eight S atoms and occur as bicapped trigonal prisms. Ln(5) and Ln/Lu sites are seven-coordinate in a monocapped trigonal prismatic arrangement. It is worth noting that Ln/LuS_7 has intermediate bond distances. For example, the average value of Ce/LuS_7 is 2.81 Å, which is between 2.91 Å for CeS_7 and 2.75 Å for LuS_7 according to the radii reported by Shannon [22]. Compared to larger lanthanides, Lu^{3+} ions have fewer S neighbors. Both Lu(1) and Lu(2) atoms are bound to six S atoms in octahedral environments. Seven-coordinate Lu(4) atoms are found to have a highly distorted monocapped trigonal prismatic geometry, with two short bonds and three long contacts. In case of δ-$Ce_{1.30}Lu_{0.70}S_3$, Lu(4)-S bond distances are 2.478(3) Å ×2, 2.690(6) Å, 3.016(6) Å, 3.304(4) Å ×2, and 3.408(5) Å. The selected bond distances are listed in Table 3.

The complex three-dimensional structure of δ-$Ln_{2-x}Lu_xS_3$ (Ln = Ce, Pr, Nd; x = 0.67 – 0.71) is constructed from one-dimensional chains of LnS_n (n = 6 – 9) polyhedra that extend along the *b* axis. Chains constructed from LnS_9 or LnS_8 polyhedra share opposite trigonal faces with two neighbors along the direction of chain propagation. The small six- and seven coordinate Ln^{3+} containing units only share edges within the chains. Each LnS_x or LuS_y polyhedra share edges and corners with others in the [*ac*] plane. They are normal compared to the Shannon's data [22].

Because there are no S–S bonds in δ-$Ln_{2-x}Lu_xS_3$ (Ln = Ce, Pr, Nd; x = 0.67 – 0.71), the oxidation states in these compounds can be assigned as +3/+3/-2. This designation is confirmed by both bond-valence sum calculations [26, 27] and by magnetic susceptibility measurements (*vide infra*).

Magnetic susceptibility. The inverse molar Ln magnetic susceptibilities for δ-$Ln_{2-x}Lu_xS_3$ (Ln = Ce, Pr, Nd; x = 0.67 – 0.71) in the range of 2-300 K are shown in Figures 2-4. All three compounds show a deviation from the Curie-Weiss law near 100 K. Magnetic parameters, which are presented in Table 6, were determined from the fit from the Curie-Weiss regions. These compounds do not show evidence of long-range magnetic ordering down to 5 K. δ-$Ce_{1.30}Lu_{0.70}S_3$ has very similar magnetic behavior with β-LnLn'S_3 [6] and γ-LnLn'S_3 [7] with a large negative value of θ_p of -34(1) K.

The $1/\chi$ data for δ-$Pr_{1.29}Lu_{0.71}S_3$ show a positive, rather than negative, deviation from Curie-Weiss behavior at 120 K. The gradual change in the slope and the negative value of θ_p (-6.0(5) K) may indicate the short-range antiferromagnetic ordering. δ-$Nd_{1.33}Lu_{0.67}S_3$ acts like a intermediate state of δ-$Ce_{1.30}Lu_{0.70}S_3$ and δ-$Pr_{1.29}Lu_{0.71}S_3$. The curvature of the plot starts as upward at 120 K. At lower temperature, it becomes negative. Crystal-field effects and short-range ordering may both contribute to this behavior. The θ_p of δ-$Nd_{1.33}Lu_{0.67}S_3$ is -8(1) K. The experimental effective magnetic moments per Ln ion based on the formulas proposed are very close to the theoretical value of the free Ln^{3+} ions as shown in Table 6. As a reference, the experimental moments using the formulas as $LnLuS_3$ (Ln = Ce, Pr, Nd) are 2.82 μ_B for $CeLuS_3$, 4.05 μ_B for $PrLuS_3$, and 3.98 μ_B for $NdLuS_3$, which are larger than the accepted values [25]. This provides further supporting evidence for the disorder refinements.

Optical properties. The UV-vis-NIR diffuse reflectance spectra are presented in Figure 5 for δ-$Ln_{2-x}Lu_xS_3$ (Ln = Ce, Pr, Nd; x = 0.67 – 0.71). The measured band gaps for δ-$Ce_{1.30}Lu_{0.70}S_3$, δ-$Pr_{1.29}Lu_{0.71}S_3$, and δ-$Nd_{1.33}Lu_{0.67}S_3$ are 1.25 eV, 1.38 eV, and 1.50 eV respectively. They are consistent with the observed colors. δ-$Ce_{1.30}Lu_{0.70}S_3$ is black, while both δ-$Pr_{1.29}Lu_{0.71}S_3$ and δ-$Nd_{1.33}Lu_{0.67}S_3$ are dark red. In addition to the observed band gap for δ-$Nd_{1.33}Lu_{0.67}S_3$, f-f transitions are also apparent in the spectrum of this compound. The band gap results are comparable to the value reported for γ-LnLn'S_3 (Ln = La, Ce; Ln' = Er, Tm, Yb) [7]. δ-$Ce_{1.30}Lu_{0.70}S_3$ has smaller band gap due to the enhanced energy of the $4f^1$ electron. Much like other mixed-lanthanide chalcogenides, the electronic structures of δ-$LnLuS_3$ are tunable based on the choice of lanthanide.

Conclusions

δ-$Ln_{2-x}Lu_xS_3$ (Ln = Ce, Pr, Nd; x = 0.67 – 0.71) were prepared using a Sb_2S_3 flux and their structures determined by single crystal X-ray diffraction. These compounds crystallize in the disordered $CeTmS_3$ structure-type. EDX analyses and magnetic measurements support the proposed formulas as δ-$Ce_{1.30}Lu_{0.70}S_3$, δ-$Pr_{1.29}Lu_{0.71}S_3$, and δ-$Nd_{1.33}Lu_{0.67}S_3$. The UV-vis-NIR diffuse reflectance measurements show these compounds to be wide band-gap semiconductors.

Acknowledgment. This work was supported by the U.S. Department of Energy under Grant DE-FG02-02ER45963 through the EPSCoR Program and by the Director, Office of Science, Office of Basic Energy Sciences, Chemical Sciences, Geosciences and Biosciences Division, U. S. Department of Energy under Contract No. AC03-76SF00098.

Funds for purchasing the UV-vis-NIR spectrometer used in these studies were provided through the Chemical Sciences, Geosciences and Biosciences Division, Office of Basic Energy Sciences, Office of Science, Heavy Elements Program, U.S. Department of Energy under Grant DE-FG02-01ER15187. JSB and ESC acknowledge support from NSF-DMR 0203532. A portion of this work was performed at the National High Magnetic Field Laboratory, which is supported by the National Science Foundation Cooperative Agreement No. DMR-0084173, by the State of Florida, and by the Department of Energy.

Auxiliary Material: Further details of the crystal structure investigation may be obtained from the Fachinformationzentrum Karlsruhe, D-76344 Eggenstein-Leopoldshafen, Germany (Fax: (+49)7247-808-666; Email: crysdata@fiz-karlsruhe.de) on quoting depository numbers CSD 417936, 417937, and 417938.

References

[1] N. Rodier, P. Laruelle, C. R. Seances Acad. Sci. Ser. *C* 270 (1970) 2127.

[2] D.J.W. Ijdo, Acta Crystallogr. B36 (1980) 2403.

[3] N. Rodier, R. Julien, V. Tien, C 39 (1983) 670.

[4] K.-J. Range, A. Gietl, U. Klement, Z. Kristallogr. 207 (1993) 147.

[5] D. Carré, P. Laruelle, Acta Crystallogr. B30 (1974) 952.

[6] K. Mitchell, R. C. Somers, F. Q. Huang, J. A. Ibers, J. Solid State Chem. 177 (2004) 709.

[7] G. B. Jin, E. S. Choi, R. P. Guertin, J. S. Brooks, T. H. Bray, C. H. Booth, T. E. Albrecht-Schmitt, Chem. Mater. 19 (2007) 567.

[8] N. Rodier, P. Laruelle, Bull. Soc. fr. de Mineral. Cristallogr. 96 (1973) 30.

[9] N. Rodier, R. L. Firor, V. Tien, M. Guittard, Mat. Res. Bull. 11(1976) 1209.

[10] N. Rodier, Bull. Soc. fr. de Mineral. Cristallogr. 96 (1973) 350.

[11] N. Rodier, P. Laruelle, Bull. Soc. fr. de Mineral. Cristallogr. 95 (1972) 548.

[12] D. Carré, P. Laruelle, Acta Crystallogr. B29 (1973) 70.

[13] N. Rodier, V. Tien, Bull. Soc. fr. de Mineral. Cristallogr. 98 (1975) 30.

[14] T. Vovan, M. Guittard, N. Rodier, Mat. Res. Bull. 14(1979) 597.

[15] M. Marezio, J.P. Remeika, P.D. Dernier, Acta Crystallogr. B26 (1970) 2008.

[16] H. Noël, J. Padiou, Acta Crystallogr. B32 (1976) 1593.

[17] T. Schleid, F. Lissner, J. Alloys Compd. 189 (1992) 69.

[18] C. M. Fang, A. Meetsma, G. A. Wiegers, J. Alloys Compd. 201 (1993) 255.

[19] C. Adolphe, Annales de Chimie (Paris), (1965) 271.

[20] G. M. Sheldrick, SHELXTL PC, Version 6.12, An Integrated System for Solving, Refining, and Displaying Crystal Structures from Diffraction Data; Siemens Analytical X-Ray Instruments, Inc.: Madison, WI 2001.

[21] G. M. Sheldrick, *SADABS* 2001, Program for absorption correction using SMART CCD based on the method of Blessing: Blessing, R. H. Acta Crystallogr. A51 (1995) 33.

[22] R. D. Shannon, Acta Crystallogr. A32 (1976) 751.

[23] L. N. Mulay, E. A. Boudreaux, Theory and Applications of Molecular Diamagnetism, Wiley–Interscience: New York, 1976.

[24] W. W. Wendlandt, H. G. Hecht, Reflectance Spectroscopy, Interscience Publishers, New York, 1966.

[25] C. Kittel, Introduction to Solid State Physics, 6th Edition, Wiley, New York, (1986).

[26] I. D. Brown, D. Altermatt, Acta Crystallogr. B41 (1985) 244.

[27] N. E. Brese, M. O'Keeffe, Acta Crystallogr. B47 (1991) 192.

Figure Captions

Figure 1. A view down the *b* axis shows the complex three-dimensional structure of δ-$Ce_{1.30}Lu_{0.70}S_3$.

Figure 2. A plot of inverse molar cerium magnetic susceptibility for δ-$Ce_{1.30}Lu_{0.70}S_3$ between 2 and 300 K. Data were taken under an applied magnetic field of 0.1 T. The straight line represents the fit to Curie-Weiss law in the range of 100-300 K.

Figure 3. Temperature dependence of the reciprocal molar praseodymium magnetic susceptibility for δ-$Pr_{1.29}Lu_{0.71}S_3$ under an applied magnetic field of 0.1 T between 2 and 300 K. The straight line represents the fit to Curie-Weiss law in the range of 100-300 K.

Figure 4. Inverse molar neodymium magnetic susceptibility vs. T for δ-$Nd_{1.33}Lu_{0.67}S_3$ under an applied magnetic field of 0.1 T between 2 and 300 K. The straight line represents the fit to Curie-Weiss law in the range of 100-300 K.

Figure 5. UV-vis diffuse reflectance spectra of δ-$Ln_{2-x}Lu_xS_3$ (Ln = Ce, Pr, Nd; x = 0.67 – 0.71).

Table 1. Crystallographic Data for δ-$Ln_{2-x}Lu_xS_3$ (Ln = Ce, Pr, Nd; x = 0.67 – 0.71).

Formula	δ-$Ce_{1.30}Lu_{0.70}S_3$	δ-$Pr_{1.29}Lu_{0.71}S_3$	δ-$Nd_{1.33}Lu_{0.67}S_3$
Fw	400.86	402.31	405.13
Color	Black	dark red	Dark red
Crystal System	monoclinic	monoclinic	monoclinic
Space group	$P2_1/m$ (No. 11)	$P2_1/m$ (No. 11)	$P2_1/m$ (No. 11)
a (Å)	11.0186(7)	10.9623(10)	10.9553(7)
b (Å)	3.9796(3)	3.9497(4)	3.9419(3)
c (Å)	21.6562(15)	21.5165(19)	21.4920(15)
β	101.6860(10)	101.579(2)	101.5080(10)
V (Å^3)	929.93(11)	912.66(15)	909.47(11)
Z	8	8	8
T (K)	193	193	193
λ (Å)	0.71073	0.71073	0.71073
ρ_{calcd} (g cm^{-3})	5.726	5.856	5.918
μ (cm^{-1})	284.95	300.82	306.04
R(F)[a]	0.0288	0.0407	0.0300
$R_w(F_o^2)$ [b]	0.0656	0.0987	0.0762

[a] $R(F) = \sum \left| |F_o| - |F_c| \right| / \sum |F_o|$ for $F_o^2 > 2\sigma(F_o^2)$. [b] $R_w\left(F_o^2\right) = \left[\sum \left[w\left(F_o^2 - F_c^2\right)^2 \right] / \sum w F_o^4 \right]^{1/2}$.

Table 2. Atomic Coordinates and Equivalent Isotropic Displacement Parameters for δ-$Ce_{1.30}Lu_{0.70}S_3$.

Atom (site)	*x*	*y*	*z*	U_{eq} (Å^2)[a]
Ce1	0.19847(5)	0.25	0.76193(3)	0.00853(13)
Ce2	0.58871(5)	0.25	0.86078(3)	0.00753(13)
Ce3	0.80925(5)	0.25	0.72906(3)	0.00609(12)
Ce4	0.69987(5)	0.25	0.53486(3)	0.00697(13)
Ce5	0.02154(10)	0.25	0.09339(5)	0.0113(2)
Lu1	0.94671(4)	0.25	0.41832(2)	0.00977(11)
Lu2	0.52820(5)	0.25	0.35266(3)	0.00965(13)
Ce/Lu	0.67261(5)	0.25	0.04880(2)	0.00988(18)
Lu4	0.0588(5)	0.25	0.0804(2)	0.0176(10)
S1	0.4135(2)	0.25	0.03938(12)	0.0088(5)
S2	0.2948(2)	0.25	0.36659(11)	0.0069(5)
S3	0.7532(2)	0.25	0.32707(12)	0.0094(5)
S4	0.8554(2)	0.25	0.96392(12)	0.0107(5)
S5	0.9936(2)	0.25	0.22765(12)	0.0089(5)
S6	0.2529(2)	0.25	0.17836(12)	0.0080(5)
S7	0.6208(2)	0.25	0.16832(12)	0.0080(5)
S8	0.1437(2)	0.25	0.51372(12)	0.0089(5)
S9	0.4433(2)	0.25	0.55520(12)	0.0109(5)
S10	0.5364(2)	0.25	0.72589(12)	0.0083(5)
S11	0.9553(2)	0.25	0.63164(12)	0.0104(5)
S12	0.1680(2)	0.25	0.89765(12)	0.0117(5)

[a] U_{eq} is defined as one-third of the trace of the orthogonalized U_{ij} tensor.

Table 3. Atomic Coordinates and Equivalent Isotropic Displacement Parameters for δ-$Pr_{1.29}Lu_{0.71}S_3$.

Atom (site)	*x*	*y*	*z*	U_{eq} (Å^2)[a]
Pr1	0.19691(8)	0.25	0.76308(4)	0.0084(2)
Pr2	0.58798(8)	0.25	0.86070(4)	0.0075(2)
Pr3	0.80815(8)	0.25	0.72974(4)	0.00628(19)
Pr4	0.69981(8)	0.25	0.53557(4)	0.00693(19)
Pr5	0.0220(4)	0.25	0.09241(17)	0.0087(4)
Lu1	0.94660(6)	0.25	0.41786(3)	0.00951(17)
Lu2	0.52939(6)	0.25	0.35258(3)	0.01012(18)
Pr/Lu	0.67394(7)	0.25	0.04788(3)	0.0094(3)
Lu4	0.051(2)	0.25	0.0793(9)	0.015(3)
S1	0.4140(4)	0.25	0.03935(19)	0.0092(8)
S2	0.2947(3)	0.25	0.36625(18)	0.0071(7)
S3	0.7549(3)	0.25	0.32577(19)	0.0090(8)
S4	0.8567(4)	0.25	0.96457(19)	0.0113(8)
S5	0.9947(3)	0.25	0.22627(19)	0.0095(8)
S6	0.2531(3)	0.25	0.17760(18)	0.0076(7)
S7	0.6222(4)	0.25	0.16747(19)	0.0090(7)
S8	0.1442(3)	0.25	0.51375(19)	0.0086(7)
S9	0.4424(4)	0.25	0.55476(19)	0.0107(8)
S10	0.5369(4)	0.25	0.72688(18)	0.0092(7)
S11	0.9543(4)	0.25	0.6323(2)	0.0111(8)
S12	0.1657(4)	0.25	0.89822(19)	0.0112(8)

[a] U_{eq} is defined as one-third of the trace of the orthogonalized U_{ij} tensor.

Table 4 Atomic Coordinates and Equivalent Isotropic Displacement Parameters for δ-$Nd_{1.33}Lu_{0.67}S_3$.

Atom (site)	*x*	*y*	*z*	U_{eq} (Å^2)[a]
Nd1	0.19518(5)	0.25	0.76324(3)	0.00894(14)
Nd2	0.58694(5)	0.25	0.85947(3)	0.00822(14)
Nd3	0.80693(5)	0.25	0.72945(3)	0.00681(13)
Nd4	0.70009(5)	0.25	0.53580(3)	0.00763(13)
Nd5	0.0234(3)	0.25	0.09212(12)	0.0082(3)
Lu1	0.94665(4)	0.25	0.41779(2)	0.01036(12)
Lu2	0.53089(4)	0.25	0.35315(2)	0.01107(13)
Nd/Lu	0.67466(5)	0.25	0.04720(2)	0.00911(19)
Lu4	0.049(2)	0.25	0.0816(10)	0.013(3)
S1	0.4146(2)	0.25	0.04108(12)	0.0094(5)
S2	0.2955(2)	0.25	0.36661(12)	0.0069(5)
S3	0.7555(2)	0.25	0.32486(13)	0.0100(5)
S4	0.8566(3)	0.25	0.96404(13)	0.0110(5)
S5	0.9960(2)	0.25	0.22621(13)	0.0094(5)
S6	0.2545(2)	0.25	0.17833(12)	0.0087(5)
S7	0.6232(2)	0.25	0.16816(12)	0.0091(5)
S8	0.1452(2)	0.25	0.51344(12)	0.0091(5)
S9	0.4426(2)	0.25	0.55385(13)	0.0115(5)
S10	0.5367(2)	0.25	0.72630(12)	0.0090(5)
S11	0.9535(3)	0.25	0.63255(13)	0.0106(5)
S12	0.1628(2)	0.25	0.89773(12)	0.0103(5)

[a] U_{eq} is defined as one-third of the trace of the orthogonalized U_{ij} tensor.

Table 5. Selected Bond Distances (Å) for δ-$Ln_{2-x}Lu_xS_3$ (Ln = Ce, Pr, Nd; x = 0.67 – 0.71).

Formula	δ- $Ce_{1.30}Lu_{0.70}S_3$	δ-$Pr_{1.29}Lu_{0.71}S_3$	δ-$Nd_{1.33}Lu_{0.67}S_3$
Ln(1)-S(3) ×2	2.8940(19)	2.870(3)	2.858(2)
Ln(1)-S(5) ×2	2.9466(19)	2.925(3)	2.918(2)
Ln(1)-S(7) ×2	2.9978(19)	2.980(3)	2.974(2)
Ln(1)-S(10)	3.957(3)	3.957(4)	3.976(3)
Ln(1)-S(11)	3.476(3)	3.462(4)	3.454(3)
Ln(1)-S(12)	3.025(3)	2.995(4)	2.981(3)
Ln(2)-S(1) ×2	2.9421(19)	2.923(3)	2.910(2)
Ln(2)-S(4)	3.312(3)	3.321(4)	3.336(3)
Ln(2)-S(6) ×2	2.8850(18)	2.862(3)	2.8507(19)
Ln(2)-S(7) ×2	3.0162(19)	3.002(3)	2.998(2)
Ln(2)-S(10)	2.861(3)	2.821(4)	2.805(3)
Ln(3)-S(2) ×2	2.9331(18)	2.916(3)	2.9122(19)
Ln(3)-S(5) ×2	2.9551(19)	2.941(3)	2.938(2)
Ln(3)-S(6) ×2	3.0007(19)	2.977(3)	2.966(2)
Ln(3)-S(10)	2.993(3)	2.962(4)	2.948(3)
Ln(3)-S(11)	2.901(3)	2.882(4)	2.872(3)
Ln(4)-S(2) ×2	2.9098(18)	2.884(3)	2.8715(19)
Ln(4)-S(8) ×2	2.9615(19)	2.946(3)	2.932(2)
Ln(4)-S(9) ×2	3.001(2)	2.982(3)	2.973(2)
Ln(4)-S(9)	2.948(3)	2.933(4)	2.923(3)
Ln(4)-S(11)	3.150(3)	3.128(4)	3.119(3)

Ln(5)-S(4) ×2	2.832(2)	2.798(5)	2.776(3)
Ln(5)-S(4)	3.022(3)	2.975(5)	2.985(4)
Ln(5)-S(5)	2.985(3)	2.955(6)	2.957(4)
Ln(5)-S(6)	2.825(3)	2.813(4)	2.823(4)
Ln(5)-S(12) ×2	2.920(2)	2.888(4)	2.876(3)
Lu(1)-S(3)	2.597(3)	2.583(4)	2.590(3)
Lu(1)-S(8) ×2	2.7771(18)	2.765(3)	2.7702(19)
Lu(1)-S(8)	2.677(3)	2.675(4)	2.678(3)
Lu(1)-S(11) ×2	2.6020(17)	2.592(3)	2.5933(17)
Lu(2)-S(2)	2.649(2)	2.647(4)	2.652(3)
Lu(2)-S(3)	2.647(3)	2.649(4)	2.649(3)
Lu(2)-S(9) ×2	2.7904(19)	2.779(3)	2.7808(19)
Lu(2)-S(10) ×2	2.6210(16)	2.618(3)	2.6160(17)
Ln/Lu-S(1) ×2	2.7880(18)	2.762(3)	2.7749(19)
Ln/Lu-S(1)	2.820(3)	2.819(4)	2.826(3)
Ln/Lu-S(4)	2.989(3)	2.944(4)	2.930(3)
Ln/Lu-S(7)	2.761(3)	2.744(4)	2.768(3)
Ln/Lu-S(12) ×2	2.7500(18)	2.742(3)	2.7595(19)
Lu(4)-S(4) ×2	2.478(3)	2.487(16)	2.513(16)
Lu(4)-S(4)	3.016(6)	2.921(15)	2.951(18)
Lu(4)-S(5)	3.408(5)	3.34(2)	3.27(2)
Lu(4)-S(6)	2.690(6)	2.736(15)	2.741(18)
Lu(4)-S(12) ×2	3.304(4)	3.20(2)	3.145(19)

Table 6. Magnetic Parameters for δ-$Ln_{2-x}Lu_xS_3$ (Ln = Ce, Pr, Nd; x = 0.67 – 0.71).

Formula	P_{cal}/μ_B	P_{eff}/μ_B	θ_p/K	R^2
δ-$Ce_{1.30}Lu_{0.70}S_3$	2.54	2.438(5)	-34(1)	0.99952
δ-$Pr_{1.29}Lu_{0.71}S_3$	3.58	3.583(4)	-6.0(5)	0.99989
δ-$Nd_{1.33}Lu_{0.67}S_3$	3.62	3.413(8)	-8(1)	0.99959

[a] P_{cal} and P_{eff} : calculated [25] and experimental effective magnetic moments per Ln ion.
[b] Weiss constant (θ_p) and goodness of fit (R^2) obtained from high temperature (100-300 K) data.

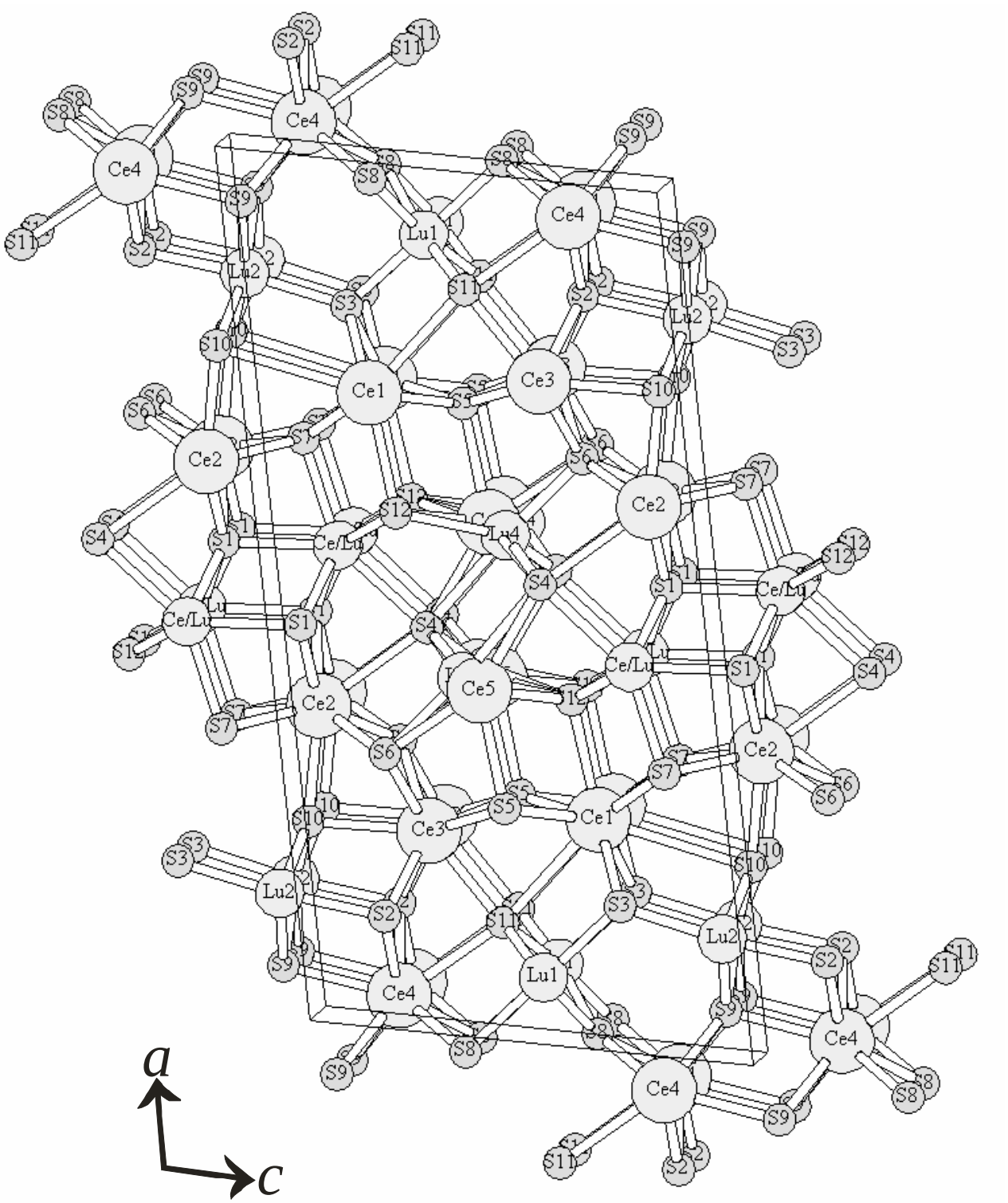
Ce4
Ce4
Ce4
Lu1
Lu2
Lu2
Ce1
Ce3
Ce2
Ce2
Ce/Lu
Ce/Lu
Ce/Lu
Ce5
Ce2
Ce2
Ce3
Ce1
Lu2
Lu2
Lu1
Ce4
Ce4
Ce4
a
c

Figure 1.

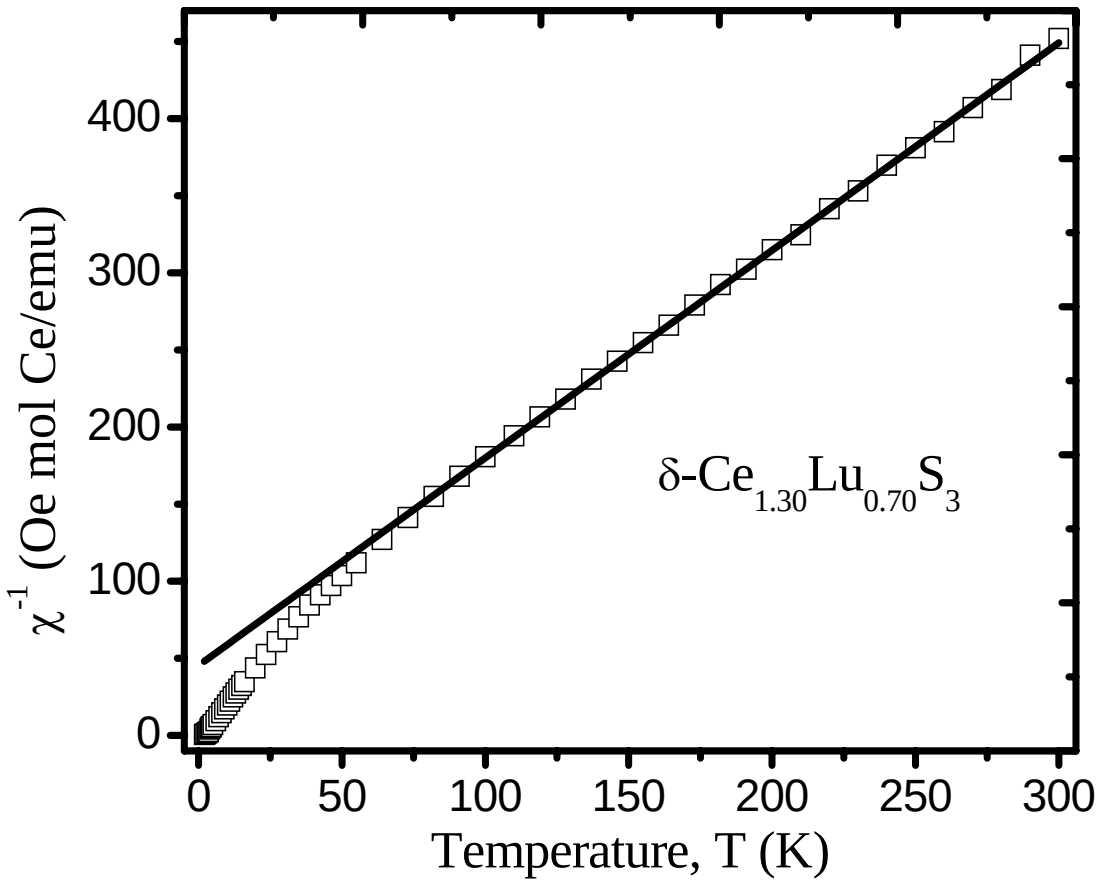
400
300
200
100
0
χ-1 (Oe mol Ce/emu)
δ-Ce1.30Lu0.70S3
0
50
100
150
200
250
300
Temperature, T (K)

Figure 2.

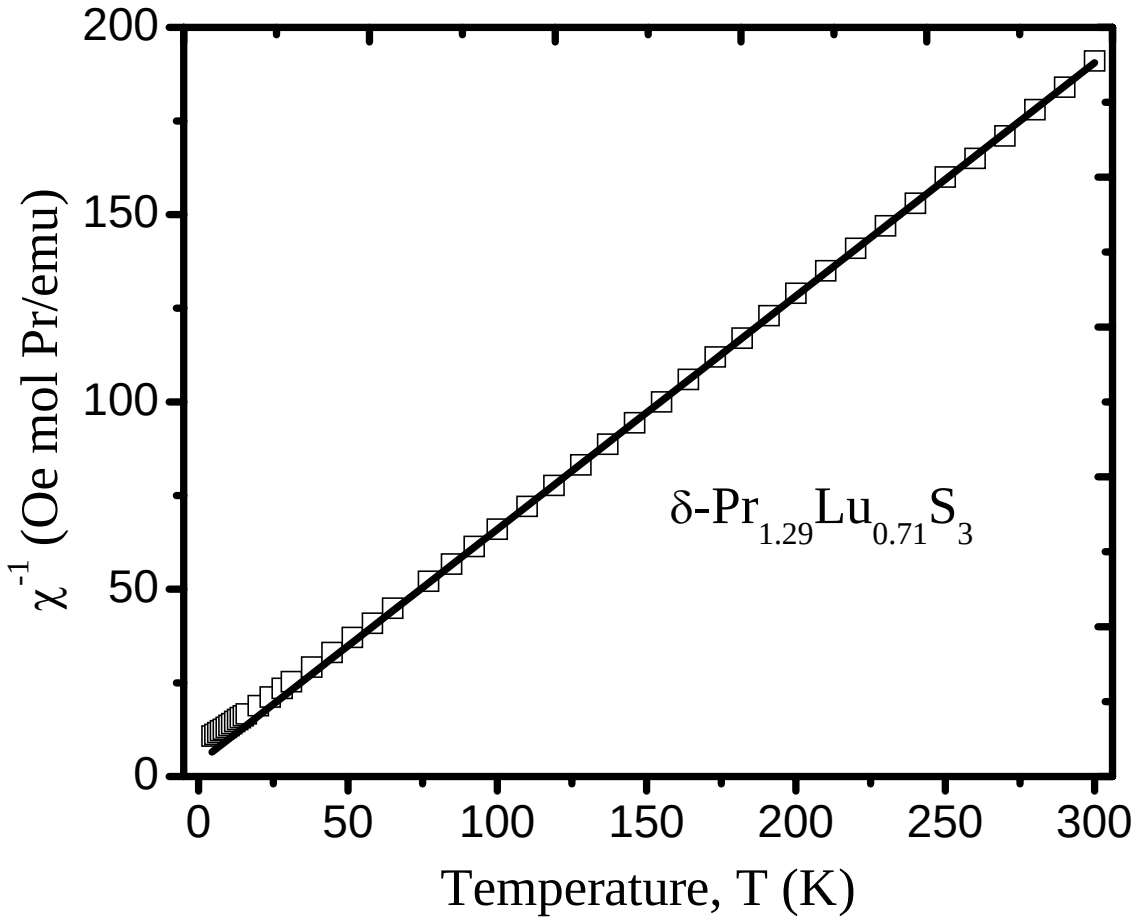
200
150
100
50
0
χ^{-1} (Oe mol Pr/emu)
δ-$Pr_{1.29}Lu_{0.71}S_3$
0
50
100
150
200
250
300
Temperature, T (K)

Figure 3.

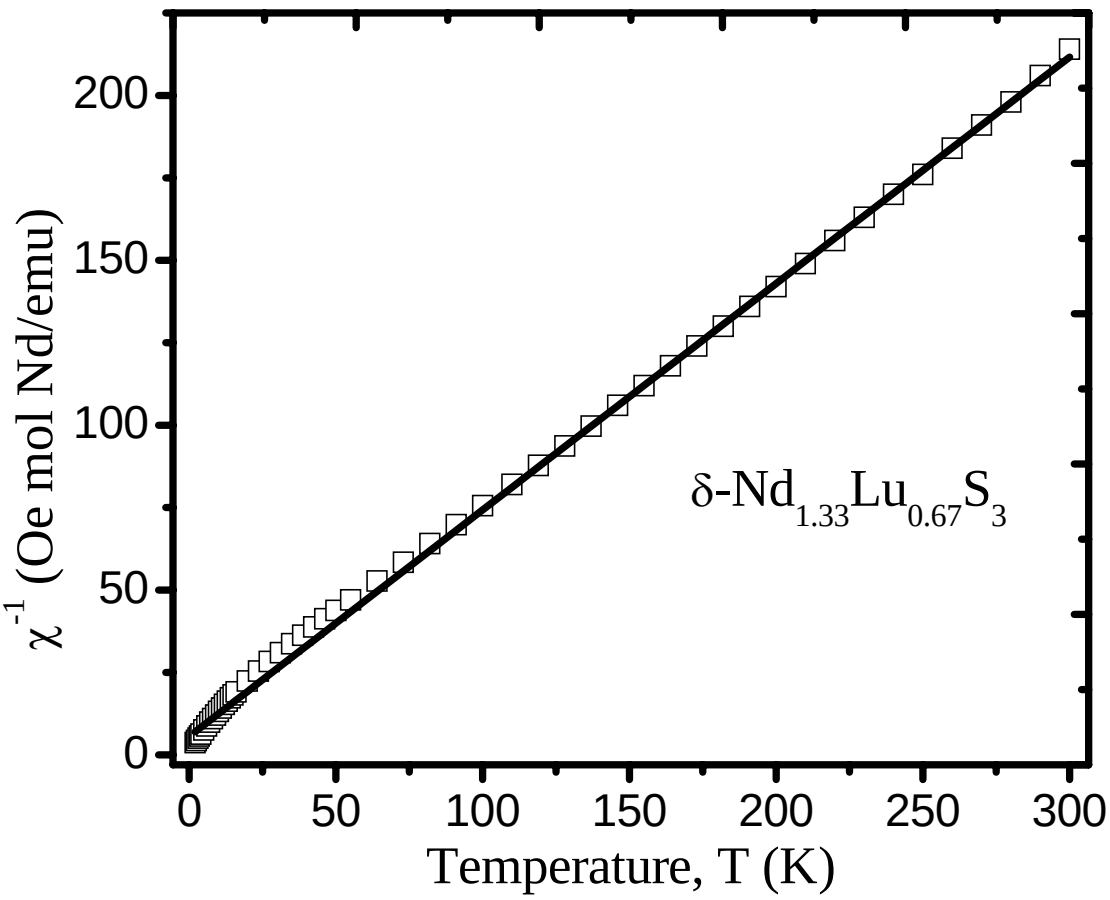
200
150
100
50
0
χ-1 (Oe mol Nd/emu)
δ-Nd1.33Lu0.67S3
0
50
100
150
200
250
300
Temperature, T (K)

Figure 4.

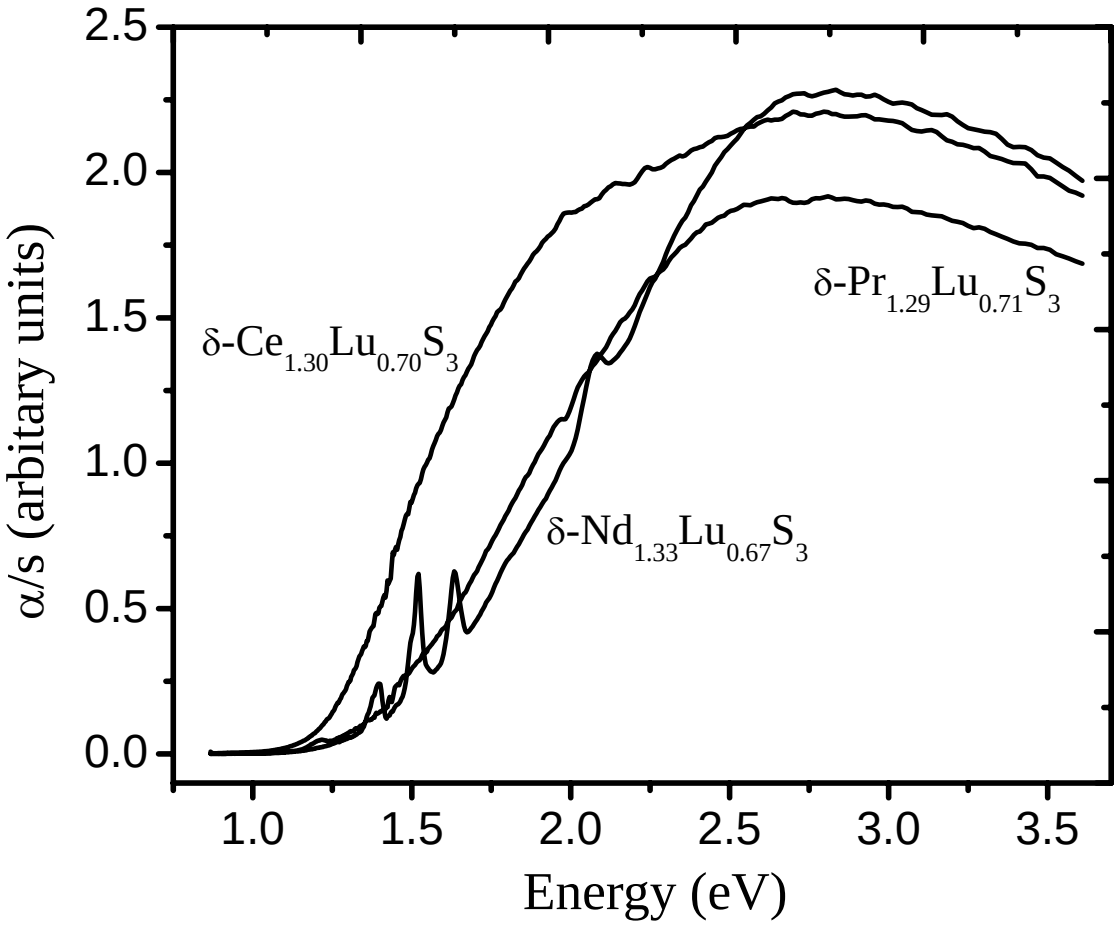
2.5
2.0
1.5
1.0
0.5
0.0
α/s (arbitary units)
δ-Ce1.30Lu0.70S3
δ-Pr1.29Lu0.71S3
δ-Nd1.33Lu0.67S3
1.0
1.5
2.0
2.5
3.0
3.5
Energy (eV)

Figure 5.